Mathematical Biosciences and Engineering

MBE, 19 (3): 2286–2309.
DOI: 10.3934/mbe.2022106
Received: 12 September 2021
Revised: 05 December 2021
Accepted: 22 December 2021
Published: 04 January 2022

http://www.aimspress.com/journal/MBE

Research article

Fixed-time sliding mode attitude control of a flexible spacecraft with rotating appendages connected by magnetic bearing

Gaowang Zhang, Feng Wang, Jian Chen and Huayi Li*

Research Center of the Satellite Technology, Harbin Institute of Technology, Harbin 150080, China

* **Correspondence:** Email: lihuayi@hit.edu.cn; Tel: + (0451)86402858; Fax: + (0451)86402858.

Abstract: This study focuses on the attitude control of a flexible spacecraft comprising rotating appendages, magnetic bearings, and a satellite platform capable of carrying flexible solar panels. The kinematic and dynamic models of the spacecraft were established using Lagrange methods to describe the translation and rotation of the spacecraft system and its connected components. A simplified model of the dynamics of a five-degrees-of-freedom (DOF) active magnetic bearing was developed using the equivalent stiffness and damping methods based on the magnetic gap variations in the magnetic bearing. Next, a fixed-time sliding mode control method was proposed for each component of the spacecraft to adjust the magnetic gap of the active magnetic bearing, realize a stable rotation of the flexible solar panels, obtain a high inertia for the appendage of the spacecraft, and accurately control the attitude. Finally, the numerical simulation results of the proposed fixed-time control method were compared with those of the proportional-derivative control method to demonstrate the superiority and effectiveness of the proposed control law.

Keywords: active magnetic bearing; fixed-time control; rotating appendages; flexible spacecraft

1. Introduction

Over the past few decades, owing to the complexity of nonlinear systems, the stabilization and reliability of such systems has been a popular research topic [1]. There are several methods for controlling nonlinear systems, such as PID control [2], anti-disturbance control [3], adaptive fuzzy control [4], robust control [5], feedback control [6], neural networks [7,8], and sliding mode control [9,10]. With the rapid development of modern space technology and the increasing complexity of space missions, low-cost spacecrafts are required to operate at high efficiencies. In the case of remote sensing

satellites, the observation width is an important indicator of their observation capability. A new type of spacecraft with a rapidly rotating payload for imaging represents a breakthrough from conventional large-satellites models. In this system, instead of increasing the payload, the payload continuously rotates to increase the observation width, effectively meeting the requirements of the spacecraft [11]. New rotating satellites are connected to the spacecraft platform and the rotating payload via frictionless magnetic bearings. The active magnetic bearings (AMBs) used in spacecrafts have several advantages over mechanical bearings, such as a lack of friction, rapid response, high speed, and high load-carrying capacity [12].

The new rotating spacecraft is a complex system with strong nonlinearity, making it important to reference nonlinear system methods to solve the control problem. There are various methods that separately study the spacecraft attitude control and maglev bearing system control problems, including PID control [13], robust adaptive control [14], adaptive backstepping control [15]and sliding mode control [16,17]. Although these control strategies can achieve good attitude control performance, most spacecraft models do not consider any magnetic bearings or rotating appendages. A few studies have been conducted on magnetic bearings that connect the rotating components to the satellite platform when carrying flexible solar panels. Wu *et al.* [18] used a new Earth observation mission spacecraft with a rotating payload as the research subject to derive the kinematic and dynamic equations for the attitude-tracking problem in the presence of an unaligned rotating payload. A chaos-based feedback control law was proposed to improve the accuracy of the angular rate. The spacecraft's angular rate accuracy was significantly improved, which was demonstrated in simulation results. Zhao *et al.* [19] analyzed a flexible spacecraft with magnetic bearings, derived the electromagnetic force of the magnetic bearings of the spacecraft using the field energy theory, and established a dynamic model of each part of the spacecraft using the virtual work principle. They analyzed the influence of the different motion states of each part on the attitude of the spacecraft. Although a new design method was proposed, it was not necessarily suitable for other complex models, and the consideration of magnetic leakage still requires improvement. Zhao *et al*. [20] established a refined dynamic model of an Earth-oriented satellite system with an unbalanced rotating payload. The interference and coupling effects of the AMB were analyzed, and simplified stiffness and damping models of the AMB were proposed. The influence of the interference term on the AMB was determined using numerical simulation. The authors showed how the refined dynamic model could effectively improve the payload working ability in the fine pointing phase. The precision model of the AMB laid the foundation for the attitude control of the spacecraft.

In this study, the existing model of the AMB was simplified by considering the rotation of a rigid appendage, rotation and vibration of flexible solar panels, and influences of a rigid rotating payload and the bearing motion on the air gap. The payload is always a high-inertia component, i.e., the appendages of a similar mass to the platform or a high-inertia matrix. A fixed-time sliding mode control strategy was proposed for a spacecraft system and verified using numerical simulation. The main contributions of this study are as follows:

1) A simplified model of a 5-DOF magnetic bearing is established, and a fixed-time sliding mode control scheme is proposed to solve the electric current signal based on the changes in the magnetic gap, so that the magnetic bearing can rapidly reach a stable state.

2) A flexible-rigid spacecraft model with a rotating payload connected using magnetic bearings is established, and a fixed-time sliding mode control law is proposed for the spacecraft platform and the rotating payload to realize the rapid and high-precision rotation of spacecraft appendages.

The remainder of this paper is organized as follows: section 2 presents the simplified Lorentz force model of a 5-DOF magnetic bearing and the dynamic and kinematic models of the spacecraft system; section 3 describes a fixed-time sliding mode control law for the spacecraft system, and the Lyapunov stability theorem is employed to validate the attitude-tracking achieved in a fixed time under the control scheme; and section 4 presents numerical simulation results, which demonstrate the effectiveness and reliability of the control strategy, and corresponding conclusions.

2. Theory: Problem formulation

2.1. Structure

A rigid-flexible coupling spacecraft model with a rotating rigid payload and flexible solar panels is described. As shown in Figure 1, the spacecraft system comprises a platform, rotating flexible panels, a rotating load, and a magnetic bearing system that connects the platform and rotating appendages. Lightweight and large-area flexible panels continuously provide energy to the spacecraft systems. The rotating appendage comprises a rotating rigid payload whose inertia is comparable to those of the platform and the momentum wheel.

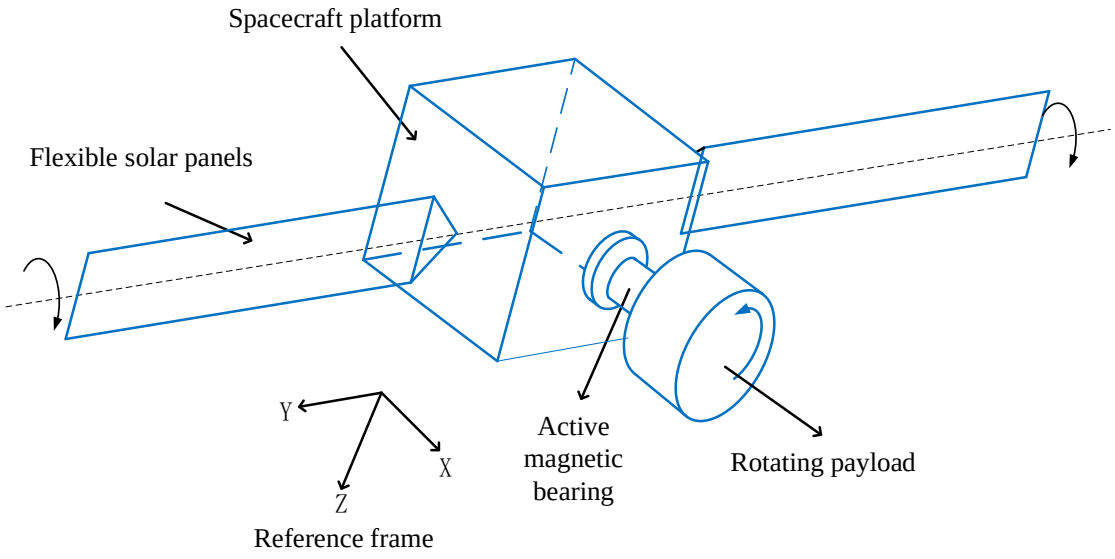

Figure 1. the structure of spacecraft system.

In the following section, a mathematical model of the rigid-flexible coupling spacecraft system is described using kinematic and dynamic equations.

2.2. Kinematic model of the spacecraft system

To avoid singularities, the kinematics of a spacecraft are often described by unit quaternions. A

unit quaternion can be expressed as $\boldsymbol{q}=\left[q_0\ \boldsymbol{q}_v^T\right]^T=\left[q_0\ q_1\ q_2\ q_3\right]^T$, where q_0 and $\boldsymbol{q}_v$ are the scalar and vector parts of the quaternion, respectively, satisfying the condition $q_0^2+\boldsymbol{q}_v^T\boldsymbol{q}_v=1$. The kinematic equation can be expressed as follows:

$$d\boldsymbol{q}=\frac{1}{2}E\left(\boldsymbol{q}\right)*\boldsymbol{\omega}, \tag{1}$$

where *E(q)* (calculated as $E(\boldsymbol{q})=\left[-\boldsymbol{q}_v^T;q_0\boldsymbol{I}+\boldsymbol{q}_v^\times\right]$) and $\boldsymbol{\omega}$ denote the angular attitude velocity of the spacecraft relative to the center of the platform and the skew-symmetric matrix of $\boldsymbol{q}_v$, respectively, such that $\boldsymbol{q}_v^\times=\left[0,-q_3,q_2;q_3,0,-q_1;-q_2,q_1,0\right]$.

To determine the attitude transformation matrix of the spacecraft, if the relative attitude quaternion of the spacecraft is expressed as $\boldsymbol{q}=\left[q_0\ q_1\ q_2\ q_3\right]^T$, we can obtain the transformation matrix from Eq (2). A direction cosine matrix can be obtained from the coordinate system '*a*' to the coordinate system '*b*,' as follows:

$$\boldsymbol{C}_{ba}=\begin{bmatrix}q_0^2+q_1^2-q_2^2-q_3^2 & 2(q_1q_2+q_0q_3) & 2(q_1q_3-q_0q_2)\\ 2(q_1q_2-q_0q_3) & q_0^2-q_1^2+q_2^2-q_3^2 & 2(q_2q_3+q_0q_1)\\ 2(q_1q_3+q_0q_2) & 2(q_2q_3-q_0q_1) & q_0^2-q_1^2-q_2^2+q_3^2\end{bmatrix}. \tag{2}$$

Thus, the formulas for the angular velocity and quaternion errors of the spacecraft platform can be defined as follows:

$$\boldsymbol{\omega}_{be}=\boldsymbol{\omega}_b-C\boldsymbol{\omega}_{bd}, \tag{3}$$

$$\boldsymbol{q}_e=\begin{bmatrix}q_{e0}\\ \boldsymbol{q}_{ev}\end{bmatrix}=\begin{bmatrix}q_0q_{d0}+\boldsymbol{q}_d^T\boldsymbol{q}_d\\ q_{d0}\boldsymbol{q}_v+\tilde{\boldsymbol{q}}_v\boldsymbol{q}_{dv}-q_0\boldsymbol{q}_{dv}\end{bmatrix}, \tag{4}$$

where $\boldsymbol{\omega}_{be}$ is the angular velocity error when the spacecraft platform is relative to the reference coordinate system, $\boldsymbol{\omega}_b$ is the actual attitude angular velocity, $\boldsymbol{\omega}_{bd}$ is the desired attitude angular velocity of the spacecraft platform relative to the spacecraft system reference frame, and $\boldsymbol{C}$ represents the transformation matrix from the actual coordinate system to the reference coordinate system.

Similarly, the angular velocity error of one-sided flexible panels can be defined as $\boldsymbol{\omega}_{ae}$, and the angle of the flexible panel relative to the *y*-axis of the spacecraft platform is $\theta_a\in\left(0,+\infty\right)$. The formula can be expressed as follows:

$$\boldsymbol{\omega}_{ae}=\boldsymbol{\omega}_a-\boldsymbol{\omega}_{ad}, \tag{5}$$

$$\boldsymbol{\theta}_a=\int \boldsymbol{\omega}_a dt, \tag{6}$$

where $\boldsymbol{\omega}_a$ is the actual attitude angular velocity, and $\boldsymbol{\omega}_{ad}$ is the desired attitude angular velocity of the flexible solar panels relative to the rotation about the *y*-axis of the spacecraft platform frame. The rotation angle (θ_{ai}) represents the i^{th} solar panel that rotates relative to the spacecraft platform. C_{ai} represents the transformation matrix from the rotation system reference frame to the fixed coordinate system of the flexible solar panel, defined as follows:

$$C_{ai}=\begin{bmatrix}\cos(\theta_{ai}) & 0 & -\sin(\theta_{ai})\\ 0 & 1 & 0\\ \sin(\theta_{ai}) & 0 & \cos(\theta_{ai})\end{bmatrix}. \tag{7}$$

Similarly, the angular velocity and rotation angle errors of the rotating appendage can be obtained.

Assumption 1: The moment of inertia of the spacecraft system has a specific form of $\boldsymbol{J}=\boldsymbol{J}_0+\Delta\boldsymbol{J}$, where $\boldsymbol{J}_0$ is the nominal constant matrix, and $\Delta\boldsymbol{J}$, which is a bounded constant, is the uncertainty in the moment of inertia.

Assumption 2 [21]: The spacecraft platform and flexible solar panels have a coupling effect, where $\delta_1\dot{\boldsymbol{\eta}}_a+\delta_2\boldsymbol{\eta}_a+\tilde{\boldsymbol{\omega}}_b\delta_3\dot{\boldsymbol{\eta}}_a$ should satisfy $\left\|\delta_1\dot{\boldsymbol{\eta}}_a+\delta_2\boldsymbol{\eta}_a+\tilde{\boldsymbol{\omega}}_b\delta_3\dot{\boldsymbol{\eta}}_a\right\|\le b_1+b_2\left\|\boldsymbol{\omega}\right\|^2$, and $b_1>0$, $b_2>0$. Thus, the inequality $\left\|\delta_1\ddot{\boldsymbol{\eta}}_a+\tilde{\boldsymbol{\omega}}\delta_3\dot{\boldsymbol{\eta}}_a\right\|\le\mu(1+\left\|\boldsymbol{\omega}\right\|^2)$ can be obtained, and $\mu=max\left(b_1,b_2\right)$.

2.3. Dynamic model of the spacecraft system

Taking into account the rotation of rigid components and flexible solar panels, we consider a rigid-flexible coupling spacecraft connected using AMBs. The Lagrange method can be applied to derive complex dynamic model equations considering the translation and rotation of the spacecraft system and the modal vibration of solar panels. The equation for the spacecraft platform can be expressed as follows:

$$M_b\ddot{\boldsymbol{X}}=-\boldsymbol{F}_c, \tag{8}$$

$$\boldsymbol{I}_b\dot{\boldsymbol{\omega}}_b+\tilde{\boldsymbol{\omega}}_b(\boldsymbol{I}_b\boldsymbol{\omega}_b+\boldsymbol{R}_{sa}\boldsymbol{\omega}_a+\boldsymbol{F}_{sa}\dot{\boldsymbol{\eta}}_a)+\boldsymbol{F}_{sa}\ddot{\boldsymbol{\eta}}_a+\boldsymbol{R}_{sa}\boldsymbol{D}_a\dot{\omega}_a=\boldsymbol{U}_b-\boldsymbol{T}_c+\boldsymbol{d}, \tag{9}$$

where M_b is the total mass of the spacecraft platform and flexible solar panels; $\boldsymbol{F}_c$ denotes the

external electromagnetic force acting on the spacecraft platform; $\boldsymbol{I}_b$ is the inertia matrix of the spacecraft, satisfying the equation $\boldsymbol{I}_b = \boldsymbol{I}_{b0} + C_{ba}\boldsymbol{I}_{a0}C_{ba}^T$; and $\boldsymbol{I}_{a0}$ denotes the inertia matrix of the flexible solar panel when it is not rotating. $\boldsymbol{U}_b$ denotes the torque of the spacecraft platform, and $\boldsymbol{d}$ is the unknown external disturbance torque. $\boldsymbol{T}_c$ denotes the projection of the resultant torque of the AMB, equivalent to the centroid of the platform. $\boldsymbol{F}_{sa}$ denotes the coupling coefficient matrix of the rotation of the spacecraft platform with the vibration of solar panels, and $\boldsymbol{F}_{sa}=\boldsymbol{F}_{+y}+\boldsymbol{F}_{-y}$. $\boldsymbol{R}_{sa}$ is the coupling coefficient matrix of the rotation between solar panels and the platform, where $\boldsymbol{R}_{sa}=\boldsymbol{R}_{+y}+\boldsymbol{R}_{-y}$ [22].

The dynamic model equations for the solar panels can be expressed as follows:

$$I_{ai}\dot{\omega}_{ai} + \boldsymbol{D}_{ai}^T\boldsymbol{F}_{ai}\ddot{\boldsymbol{\eta}}_{ai} + \boldsymbol{D}_{ai}^T\boldsymbol{R}_{sai}^T\dot{\boldsymbol{\omega}}_b = U_{ai}(i=-y,y), \tag{10}$$

$$\ddot{\boldsymbol{\eta}}_{ai} + 2\boldsymbol{\zeta}_{ai}\boldsymbol{\Omega}_{ai}\dot{\boldsymbol{\eta}}_{ai} + \boldsymbol{\Lambda}_{ai}\boldsymbol{\eta}_{ai} + \boldsymbol{F}_{sa}^T\dot{\boldsymbol{\omega}}_b + \boldsymbol{F}_{ai}^T\boldsymbol{D}\dot{\omega}_{ai} = 0(i=-y,+y) \quad , \tag{11}$$

where i denotes the i^{th} solar panel installed on the platform, I_a denotes the inertia matrix of the flexible solar panel, U_a denotes the torque originating from the control motor of the flexible solar panel, η_a denotes the modal coordinates of the solar panel, $\boldsymbol{\Omega}_a$ denotes the diagonal matrix of the modal frequency of the solar panel, $\boldsymbol{\Lambda}_a$ denotes the stiffness matrix of the solar panel such that $\boldsymbol{\Lambda}_a=\boldsymbol{\Omega}_a^2$, and $\boldsymbol{\zeta}_a$ is the damping ratio of the solar panel [22]. Notably, these parameters are diagonal matrices.

The dynamic model equations for the rotation appendage can be expressed as follows:

$$M_p\ddot{\boldsymbol{X}}_p = \boldsymbol{F}_c, \tag{12}$$

$$\boldsymbol{I}_{\mathrm{p}}\dot{\boldsymbol{\omega}}_p + \tilde{\boldsymbol{\omega}}_p\boldsymbol{I}_{\mathrm{p}}\boldsymbol{\omega}_p = \boldsymbol{U}_p + \boldsymbol{T}_c, \tag{13}$$

where I_p denotes the inertia matrix of the rigid rotation payload, and $\boldsymbol{U}_p$ denotes the torque that originates from the momentum wheel. $\boldsymbol{\omega}_p$ is the actual attitude angular velocity, and $\boldsymbol{\omega}_{pd}$ is the desired attitude angular velocity of the rotating appendage relative to the rotation about the x-axis of the

spacecraft platform reference frame.

In this study, $\boldsymbol{q}_b$ is the actual attitude quaternion, and $\boldsymbol{q}_{bd}$ is the desired quaternion of the spacecraft platform relative to the spacecraft system reference frame. $\boldsymbol{q}_a$ is the actual quaternion, and $\boldsymbol{q}_{ad}$ is the desired quaternion of flexible solar panels. $\boldsymbol{q}_p$ is the actual quaternion, and $\boldsymbol{q}_{pd}$ is the desired quaternion of the rotating appendage. $\boldsymbol{F}_{sa}$ and $\boldsymbol{R}_{sa}$ are the coefficient matrices related to the rotation angle of appendages relative to the spacecraft platform. The calculation of $\boldsymbol{F}_{sa}$ is used as an example for illustration. We assume that flexible solar panels are fixed on the *y*-axis of the spacecraft platform and rotate relative to the *y*-axis of the spacecraft system coordinate system, with the rotation angle being defined as θ_{ay}. The calculation of $\boldsymbol{F}_{sa}$ can be expressed as follows [23]:

$$\boldsymbol{F}_{sa}=\left[f_{sa1}\begin{bmatrix}\sin(\theta_{ay})\\1\\\cos(\theta_{ay})\end{bmatrix},f_{sa2}\begin{bmatrix}\sin(\theta_{ay})\\1\\\cos(\theta_{ay})\end{bmatrix},\ldots,f_{san}\begin{bmatrix}\sin(\theta_{ay})\\1\\\cos(\theta_{ay})\end{bmatrix}\right]. \tag{14}$$

Regardless of the number of flexible solar panels installed on the spacecraft platform, their rotation states relative to the platform remain the same. Therefore, the angular velocity of flexible solar panels can be defined as ω_a. Based on the equations for the translation and rotation of the platform and the rotation and vibration of flexible solar panels, the following equations can be obtained:

$$\begin{aligned}&\begin{bmatrix}\boldsymbol{I}_b-\boldsymbol{F}_{sa}\boldsymbol{F}_{sa}^T+(\boldsymbol{F}_{sa}\boldsymbol{F}_a^T-\boldsymbol{R}_{sa})\boldsymbol{D}_a(I_a-\boldsymbol{D}_a^T\boldsymbol{F}_a\boldsymbol{F}_a^T\boldsymbol{D}_a)^{-1}\boldsymbol{D}_a^T(\boldsymbol{R}_{sa}^T-\boldsymbol{F}_a\boldsymbol{F}_{sa}^T) & 0\\ \boldsymbol{D}_a^T(\boldsymbol{R}_{sa}^T-\boldsymbol{F}_a\boldsymbol{F}_{sa}^T) & (I_a-\boldsymbol{D}_a^T\boldsymbol{F}_a\boldsymbol{F}_a^T\boldsymbol{D}_a)\end{bmatrix}\begin{bmatrix}\dot{\boldsymbol{\omega}}_b\\\dot{\omega}_a\end{bmatrix}\\&+\begin{bmatrix}\tilde{\boldsymbol{\omega}}_b(\boldsymbol{I}_b\boldsymbol{\omega}_b+\boldsymbol{R}_{sa}\boldsymbol{D}_a\boldsymbol{\omega}_a+\boldsymbol{F}_{sa}\dot{\boldsymbol{\eta}}_a)\\0\end{bmatrix}=\begin{bmatrix}\boldsymbol{U}_b-\boldsymbol{T}_c+\boldsymbol{d}\\0\end{bmatrix}+\begin{bmatrix}(\boldsymbol{F}_{sa}\boldsymbol{F}_a^T-\boldsymbol{R}_{sa})\boldsymbol{D}_a(I_a-\boldsymbol{D}_a^T\boldsymbol{F}_a\boldsymbol{F}_a^T\boldsymbol{D}_a)^{-1}\\1\end{bmatrix}U_a\\&+\begin{bmatrix}\boldsymbol{F}_{sa}-(\boldsymbol{R}_{sa}-\boldsymbol{F}_{sa}\boldsymbol{F}_a^T)\boldsymbol{D}_a(I_a-\boldsymbol{D}_a^T\boldsymbol{F}_a\boldsymbol{F}_a^T\boldsymbol{D}_a)^{-1}\boldsymbol{D}_a^T\boldsymbol{F}_a\\\boldsymbol{D}_a^T\boldsymbol{F}_a\end{bmatrix}(2\zeta_a\boldsymbol{\Omega}_a\dot{\boldsymbol{\eta}}_a+\boldsymbol{\Lambda}_a\boldsymbol{\eta}_a)\end{aligned}. \tag{15}$$

It is further assumed that $\boldsymbol{J}_b=\boldsymbol{I}_b-\boldsymbol{F}_{sa}\boldsymbol{F}_{sa}^T+(\boldsymbol{F}_{sa}\boldsymbol{F}_a^T-\boldsymbol{R}_{sa})\boldsymbol{D}_a(I_a-\boldsymbol{D}_a^T\boldsymbol{F}_a\boldsymbol{F}_a^T\boldsymbol{D}_a)^{-1}\boldsymbol{D}_a^T(\boldsymbol{R}_{sa}^T-\boldsymbol{F}_a\boldsymbol{F}_{sa}^T)$, $\vartheta_\eta=2\zeta_a\boldsymbol{\Omega}_a\dot{\boldsymbol{\eta}}_a+\boldsymbol{\Lambda}_a\boldsymbol{\eta}_a$, and $\boldsymbol{H}_a=(\boldsymbol{R}_{sa}-\boldsymbol{F}_{sa}\boldsymbol{F}_a^T)\boldsymbol{D}_a(I_a-\boldsymbol{D}_a^T\boldsymbol{F}_a\boldsymbol{F}_a^T\boldsymbol{D}_a)^{-1}$, and so Eq (15) can be rewritten as:

$$\begin{bmatrix} \boldsymbol{J}_b & 0 \\ \boldsymbol{D}_a^T(\boldsymbol{R}_{sa}^T - \boldsymbol{F}_a\boldsymbol{F}_{sa}^T) & J_a \end{bmatrix}\begin{bmatrix} \dot{\boldsymbol{\omega}}_b \\ \dot{\omega}_a \end{bmatrix} + \begin{bmatrix} \tilde{\boldsymbol{\omega}}_b(\boldsymbol{I}_b\boldsymbol{\omega}_b + \boldsymbol{R}_{sa}\boldsymbol{D}_a\boldsymbol{\omega}_a + \boldsymbol{F}_{sa}\dot{\boldsymbol{\eta}}_a) \\ 0 \end{bmatrix} = \begin{bmatrix} \boldsymbol{U}_b - \boldsymbol{T}_c + \boldsymbol{d} - \boldsymbol{H}_a U_a \\ U_a \end{bmatrix}, \quad (16)$$
$$- \begin{bmatrix} \boldsymbol{H}_a\boldsymbol{D}_a^T\boldsymbol{F}_a - \boldsymbol{F}_{sa} \\ \boldsymbol{D}_a^T\boldsymbol{F}_a \end{bmatrix}\boldsymbol{\vartheta}_\eta$$

$$\dot{\boldsymbol{\omega}}_e = \begin{bmatrix} \dot{\boldsymbol{\omega}}_{be} \\ \dot{\omega}_{ae} \end{bmatrix} = \begin{bmatrix} \boldsymbol{J}_b & 0 \\ \boldsymbol{D}_a^T(\boldsymbol{R}_{sa}^T - \boldsymbol{F}_a\boldsymbol{F}_{sa}^T) & J_a \end{bmatrix}^{-1} \left\{ \begin{bmatrix} \boldsymbol{U}_b - \boldsymbol{T}_c + \boldsymbol{d} - \boldsymbol{H}_a U_a \\ U_a \end{bmatrix} \right.$$
$$\left. - \begin{bmatrix} (\boldsymbol{H}_a\boldsymbol{D}_a^T\boldsymbol{F}_a - \boldsymbol{F}_{sa})\boldsymbol{\vartheta}_\eta + \tilde{\boldsymbol{\omega}}_b\boldsymbol{F}_{sa}\dot{\boldsymbol{\eta}}_a \\ \boldsymbol{D}_a^T\boldsymbol{F}_a\boldsymbol{\vartheta}_\eta \end{bmatrix} - \begin{bmatrix} \boldsymbol{J}_b(C\dot{\boldsymbol{\omega}}_{bd} - \tilde{\boldsymbol{\omega}}_{be}C\boldsymbol{\omega}_{bd}) + \tilde{\boldsymbol{\omega}}_b(\boldsymbol{I}_b\boldsymbol{\omega}_b + \boldsymbol{R}_{sa}\boldsymbol{D}_a\boldsymbol{\omega}_a) \\ J_a\dot{\boldsymbol{\omega}}_{ad} \end{bmatrix} \right\}. \quad (17)$$

Assumption 3: For the spacecraft system, external disturbances $\boldsymbol{d}(t)$ include the gravity-gradient, solar radiation, aerodynamic, and magnetic disturbance torques [24]. The following implications can be drawn.

1) The gravity-gradient torque of flexible spacecraft in orbit is related to the initial angular velocity, inertia, and attitude angle.
2) The solar radiation torque is independent of the orbital height and is approximately constant if the orbital height is less than 500 km. The solar radiation torque is ignored in this study.
3) The aerodynamic torque results from the spacecraft motion through the tenuous upper atmosphere. The aerodynamic torque is related to the atmospheric density, drag coefficient, spacecraft velocity, area of the spacecraft cross-section, offset from the center of mass to the center of pressure, etc. This is always a small constant [25].
4) The geomagnetic field with residual magnetic field of the spacecraft produce magnetic disturbance torques. The magnetic disturbance torque can be calculated as $\boldsymbol{T} = \boldsymbol{M} \times \boldsymbol{B}$, where $\boldsymbol{M}$ is the sum of the individual magnetic moments caused by permanent and induced magnetism, and $\boldsymbol{B}$ is the geocentric magnetic flux density. Although the magnetic torque is a small parameter, it cannot be ignored.

Based on this assumption, it is assumed that the lumped external disturbance torque of the spacecraft is bounded, i.e., $\|d\| \le d_1$, and $d_1 > 0$.

2.4. Model of magnetic bearing

Figure 2 shows the simplified structure of the magnetic bearing, which includes two radial bearings, one axial bearing, and position sensors. Radial bearings are symmetrically distributed at both ends of the axial bearing [26,27]. The magnetic force of the bearing is generated by the magnetic poles at each end, where the magnetic force of each pole is related to the size of the magnetic gap, coil current, number of coil turns, and cross-sectional area of the magnet. After the gap changes in each magnetic pole pair are detected by position sensors, the current in each magnetic pole is adjusted by controllers, and the electromagnetic force is adjusted to eliminate gap changes.

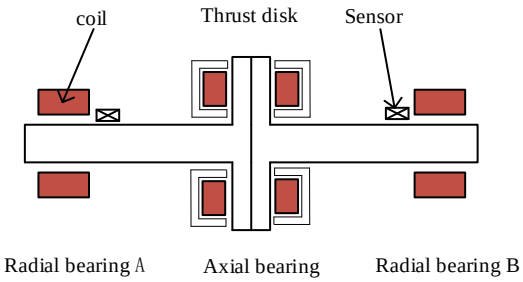

Figure 2. the simplified structure of magnetic bearing system.

We assume that the magnetic field is evenly distributed at the position of the electromagnet and the air gap, and ignoring the magnetic flux leakage and hysteresis of the magnetic bearing, the formula for the simplified model of the magnetic bearing can be expressed as follows [20]:

$$F = k\frac{i^2}{x^2} \tag{18}$$

When the structure of the magnetic bearing is determined, k is a constant value, and the magnetic bearing force is only related to the current and the air gap, being directly proportional to the square of the coil current and inversely proportional to the square of the air gap [28].The magnetic poles of the bearing are often installed in pairs, and differential control is often applied in the control mode. Because the nonlinearity of the electromagnetic force affects control, the first-order linearized electromagnetic force model can be obtained by linearizing Eq. (18), as follows:

$$F(i,x) = F(i_0,x_0) + k_i(i-i_0) - k_x(x-x_0) \tag{19}$$

where k_i (calculated as $k_i = \frac{\mu_0 N^2 A i_0}{2x_0^2}$) is the current stiffness and k_x (calculated as $k_x = -\frac{\mu_0 N^2 A i_0^2}{2x_0^3}$) is the displacement stiffness. The total force on the magnetic pole is obtained as:

$$F = 2k_i\Delta i + 2k_x\Delta x \tag{20}$$

If the Euler angle of the *zyx* rotation order is used to describe the attitude of the AMB rotor relative to the spacecraft platform, the direction cosine matrix can be expressed as follows:

$$C_{bc} = \begin{bmatrix} C\theta C\psi & C\theta C\psi & -S\theta \\ -C\varphi S\psi + S\varphi S\theta C\psi & C\varphi C\psi + S\varphi S\theta S\psi & S\varphi C\theta \\ S\varphi S\psi + C\varphi S\theta C\psi & -S\varphi S\psi + C\varphi S\theta S\psi & C\varphi C\theta \end{bmatrix} \tag{21}$$

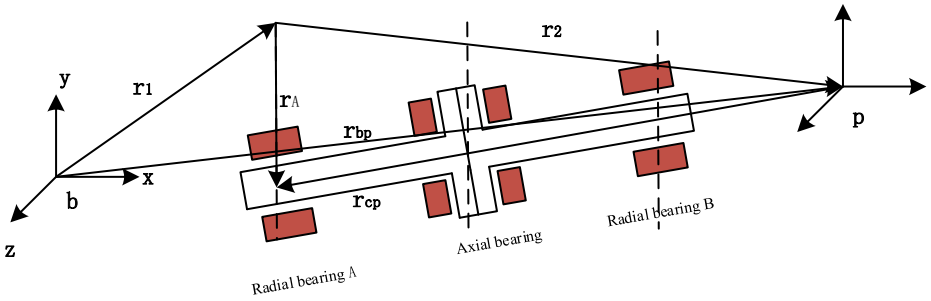

Figure 3. Diagram of magnetic gap change of radial bearing.

Figure 3 shows the magnetic gap variation in the radial bearing A, relative position variation in the spacecraft platform, and rotating payload. The *y*- and *z*-axis magnetic gap variations calculated using the simplified model of the magnetic bearing can be expressed as follows:

$$\begin{aligned} r_{Ay} &= -\frac{C_{bc}(1,2)}{C_{bc}(1,1)} * r_{2x} + r_{2y} \\ r_{Az} &= -\frac{C_{bc}(1,3)}{C_{bc}(1,1)} * r_{2x} + r_{2z} \end{aligned} \tag{22}$$

Similarly, the magnetic gap in the radial bearing B can be expressed as follows:

$$\begin{aligned} r_{By} &= -\frac{C_{bc}(1,2)}{C_{bc}(1,1)} * (r_{2x} - r_{AB}) + r_{2By} \\ r_{Bz} &= -\frac{C_{bc}(1,3)}{C_{bc}(1,1)} * (r_{2x} - r_{AB}) + r_{2Bz} \end{aligned} \tag{22}$$

The magnetic gap in the axial bearing in the *x*-direction can be obtained based on the simplified model of the magnetic bearing, as follows:

$$r_x = r_{bpx} - r_{zx} - r_{zp} * C_{bc}(1,1) \tag{23}$$

In this study, the current is determined based on the changes in the magnetic gap. A fixed-time sliding mode control method can be used to calculate the control current owing to the magnetic gap, as follows:

$$s = \Delta\dot{x} + sig(c_1 * sig(\Delta\dot{x}) + c_2 * \Delta x + c_3 * \Delta x^3)^{0.5} \tag{25}$$

$$\Delta i = -k_\alpha s - k_\beta sat(s) \tag{26}$$

3. Materials and methods: Controller design

3.1. Introduction to lemma

We introduce some concepts and lemmas which are utilized in the design of the attitude controller before delivering the main results.

Consider the nonlinear system:

$$\dot{x}(t) = f(x(t)), x(0) = 0, f(0) = 0, \tag{27}$$

where $x \in R^n$ and f are nonlinear continuous functions, which become continuous in an open neighborhood of the origin $x = 0$.

Lemma 1 [29]. For the system of Eq (27), we assume that there is a continuous differential Lyapunov function ($V(x)$) defined in its neighborhood of origin, as follows:

$$\dot{V}(x) + (\lambda_1 V^p(x) + \lambda_2 V^g(x))^k \le 0, \tag{28}$$

where α, β, p, g, $k \in R^+$, $pk < 1$, and $gk > 1$. The system can then reach $V(x) \equiv 0$ in a fixed time, and its convergence time (T) can be expressed as follows:

$$T \le \frac{1}{\lambda_1^k(1-pk)} + \frac{1}{\lambda_2^k(gk-1)}. \tag{29}$$

Lemma 2 [30]. For any $x_i \in R(i = 1, 2, ..., n)$ and a positive number $\gamma \in (0, 1)$, the following inequality holds:

$$\left(\sum_{i=1}^{n} |x_i|^2\right)^{\frac{1+\gamma}{2}} \le \sum_{i=1}^{n} |x_i|^{1+\gamma}, \tag{30}$$

$$(|x_1| + |x_2| + \cdots |x_n|)^p \le |x_1|^p + |x_2|^p + \cdots |x_n|^p. \tag{31}$$

Lemma 3 [31]. For any $x \in R^n$, $a \in R$, the following operations hold:

$$\frac{d|x|^{\gamma+1}}{dt} = (\gamma+1)diag(sig(x)^{\gamma})\dot{x}, \tag{32}$$

$$\frac{dsig(x)^{\gamma+1}}{dt} = (\gamma+1)diag(|x|)^{\gamma})\dot{x}\,. \tag{33}$$

3.2. Controller design of platform and flexible solar panels

We suppose $\boldsymbol{q}_e = \begin{bmatrix}\boldsymbol{q}_{be} & \boldsymbol{q}_{ae}\end{bmatrix}^T$, $\dot{\boldsymbol{q}}_e = \begin{bmatrix}\dot{\boldsymbol{q}}_{be} & \dot{\boldsymbol{q}}_{ae}\end{bmatrix}^T = \frac{1}{2}\boldsymbol{E}\boldsymbol{\omega}_e$, and $\boldsymbol{E} = \begin{bmatrix}\boldsymbol{E}(\boldsymbol{q}_e) & 0\\ 0 & \boldsymbol{E}(\boldsymbol{q}_{ae})\end{bmatrix}$,

$$\ddot{\boldsymbol{q}}_e = \begin{bmatrix}-\frac{1}{4}\boldsymbol{q}_{be}\omega_{be}^T\omega_{be} + \frac{1}{2}E(\boldsymbol{q}_{be})\dot{\omega}_{be}\\ -\frac{1}{4}\boldsymbol{q}_{ae}\omega_{ae}^T\omega_{ae} + \frac{1}{2}E(\boldsymbol{q}_{ae})\dot{\omega}_{ae}\end{bmatrix} = -\frac{1}{4}L + \frac{1}{2}E(\boldsymbol{q}_e)\dot{\omega}_e\,.$$

Based on the fixed-time sliding surface designed in [32], the following fixed-time sliding surface can be considered in this study:

$$\boldsymbol{S}_e = \boldsymbol{\omega}_e + sig(\boldsymbol{k}_1 * sig^p(\dot{\boldsymbol{q}}_e) + \boldsymbol{k}_2 * \boldsymbol{q}_e^{\,m} + \boldsymbol{k}_3 * \boldsymbol{q}_e^{\,n})^q\,, \tag{34}$$

where $\boldsymbol{k}_1$, $\boldsymbol{k}_2$, and $\boldsymbol{k}_3$ are the parameter matrices, and $\boldsymbol{k}_1 = \mathrm{diag}(k_{11}, k_{12}, k_{13}, k_{14})$, $\boldsymbol{k}_2 = \mathrm{diag}(k_{21}, k_{22}, k_{23}, k_{24})$, and $\boldsymbol{k}_3 = \mathrm{diag}(k_{31}, k_{32}, k_{33}, k_{34})$, where $mq < 1$, and $nq > 1$.

It can be defined as $\boldsymbol{x} = qdiag(|\boldsymbol{k}_1 sig^2(\dot{\boldsymbol{q}}_e) + \boldsymbol{k}_2\boldsymbol{q}_e^m + \boldsymbol{k}_3\boldsymbol{q}_e^n|^{q-1})$, and $\boldsymbol{J} = \begin{bmatrix}\boldsymbol{J}_b & \\ & J_a\end{bmatrix}$. Once the sliding surface has been designed, a fixed-time control law ($\boldsymbol{U}$) can be designed, as follows:

$$\boldsymbol{U} = \begin{bmatrix}\boldsymbol{U}_b\\ U_a\end{bmatrix} = \boldsymbol{U}_1 + \boldsymbol{U}_2\,, \tag{35}$$

$$\boldsymbol{U}_1 = \begin{bmatrix}\boldsymbol{T}_c - \boldsymbol{d} + \boldsymbol{H}_a U_a + \mu(1+\|\boldsymbol{\omega}\|^2) + \boldsymbol{J}_b(C\dot{\boldsymbol{\omega}}_{bd} - \tilde{\boldsymbol{\omega}}_{be}C\boldsymbol{\omega}_{bd}) + \tilde{\boldsymbol{\omega}}_b(\boldsymbol{I}_b\boldsymbol{\omega}_b + \boldsymbol{R}_{sa}\boldsymbol{D}_a\boldsymbol{\omega}_a)\\ \boldsymbol{D}_a^T\boldsymbol{F}_a\vartheta_\eta + J_a\dot{\omega}_{ad} + \boldsymbol{D}_a^T(\boldsymbol{R}_{sa}^T - \boldsymbol{F}_a\boldsymbol{F}_{sa}^T)\dot{\boldsymbol{\omega}}_b\end{bmatrix}, \tag{36}$$

$$\begin{aligned}\boldsymbol{U}_2 = \boldsymbol{J}\Big[\boldsymbol{E}_4 + \boldsymbol{x}\cdot\boldsymbol{k}_1\cdot diag(|\dot{\boldsymbol{q}}_e|)\boldsymbol{E}\Big]^{-1}\Big\{&q\boldsymbol{x}\cdot\boldsymbol{k}_1\cdot diag(|\dot{\boldsymbol{q}}_e|)\boldsymbol{L}\\ &-q\boldsymbol{x}(m\boldsymbol{k}_2 + n\boldsymbol{k}_3)diag(|\boldsymbol{q}_e^{\,m-1}|)\dot{\boldsymbol{q}}_e - \Big[\boldsymbol{k}_4 sig^{2k_5}(\boldsymbol{S}) + \boldsymbol{k}_6 sig^{2k_7}(\boldsymbol{S})\Big]^q\Big\}\,.\end{aligned} \tag{37}$$

A fixed-time sliding mode surface and a control law are proposed with the spacecraft attitude dynamic model established in this study. The system state slides to the equilibrium point at a fixed time. We consider the candidate Lyapunov function as follows [33]:

$$V = \frac{1}{2}\boldsymbol{S}^T\boldsymbol{S}. \tag{38}$$

Because

$$\dot{\boldsymbol{S}} = \dot{\boldsymbol{\omega}}_e + \boldsymbol{x}\left[2\boldsymbol{k}_1 \cdot diag(|\dot{\boldsymbol{q}}_e|)\ddot{\boldsymbol{q}}_e + m\boldsymbol{k}_2 diag(|\boldsymbol{q}_e|^{m-1})\dot{\boldsymbol{q}}_e + n\boldsymbol{k}_3 diag(|\boldsymbol{q}_e|^{n-1})\dot{\boldsymbol{q}}_e\right], \tag{39}$$

the derivatives of V along the trajectory of the spacecraft system can be obtained by substituting (39) into the Eq (38), as follows:

$$\begin{aligned}
\dot{V} &= \boldsymbol{S}^T\dot{\boldsymbol{S}} \\
&= \boldsymbol{S}^T\left\{\dot{\boldsymbol{\omega}}_e + \boldsymbol{x}\left[2\boldsymbol{k}_1 \cdot diag(|\dot{\boldsymbol{q}}_e|)\ddot{\boldsymbol{q}}_e + m\boldsymbol{k}_2 diag(|\boldsymbol{q}_e^{m-1}|)\dot{\boldsymbol{q}}_e + n\boldsymbol{k}_3 diag(|\boldsymbol{q}_e^{n-1}|)\dot{\boldsymbol{q}}_e\right]\right\} \\
&= \boldsymbol{S}^T\left\{\dot{\boldsymbol{\omega}}_e + 2\boldsymbol{x}\cdot\boldsymbol{k}_1 \cdot diag(|\dot{\boldsymbol{q}}_e|)\left[-\frac{1}{4}\boldsymbol{L} + \frac{1}{2}E(\boldsymbol{q}_e)\dot{\boldsymbol{\omega}}_e\right]\right. \\
&\quad \left. + \boldsymbol{q}\boldsymbol{x}\left[m\boldsymbol{k}_2 diag(|\boldsymbol{q}_e^{m-1}|)\dot{\boldsymbol{q}}_e + n\boldsymbol{k}_3 diag(|\boldsymbol{q}_e^{n-1}|)\dot{\boldsymbol{q}}_e\right]\right\} \\
&= \boldsymbol{S}^T\left\{\begin{array}{l}
\left[\boldsymbol{E}_4 + \boldsymbol{x}\cdot\boldsymbol{k}_3 \cdot diag(|\dot{\boldsymbol{q}}_e|)\boldsymbol{E}\right]\boldsymbol{J}^{-1}\left\{\begin{bmatrix}\boldsymbol{U}_b - \boldsymbol{T}_c + \boldsymbol{d} - \boldsymbol{H}_a U_a \\ U_a\end{bmatrix}\right. \\
-\begin{bmatrix}(\boldsymbol{H}_a\boldsymbol{D}_a^T\boldsymbol{F}_a - \boldsymbol{F}_{sa})\boldsymbol{\vartheta}_\eta + \tilde{\boldsymbol{\omega}}_b\boldsymbol{F}_{sa}\dot{\boldsymbol{\eta}}_a \\ \boldsymbol{D}_a^T\boldsymbol{F}_a\boldsymbol{\vartheta}_\eta\end{bmatrix} \\
\left.-\begin{bmatrix}\boldsymbol{J}_b(C\dot{\boldsymbol{\omega}}_{bd} - \tilde{\boldsymbol{\omega}}_{be}C\boldsymbol{\omega}_{bd}) + \tilde{\boldsymbol{\omega}}_b(\boldsymbol{I}_b\boldsymbol{\omega}_b + \boldsymbol{R}_{sa}\boldsymbol{D}_a\boldsymbol{\omega}_a) \\ J_a\dot{\boldsymbol{\omega}}_{ad}\end{bmatrix}\right\} \\
-\frac{1}{2}\boldsymbol{x}\cdot\boldsymbol{k}_1 \cdot diag(|\dot{\boldsymbol{q}}_e|)\boldsymbol{L} + q\boldsymbol{x}\left[m\boldsymbol{k}_2 diag(|\boldsymbol{q}_e^{m-1}|)\dot{\boldsymbol{q}}_e + n\boldsymbol{k}_3 diag(|\boldsymbol{q}_e^{n-1}|)\dot{\boldsymbol{q}}_e\right]
\end{array}\right\} \\
&\le \boldsymbol{S}^T\left\{\left[\boldsymbol{E}_4 + \boldsymbol{x}\cdot\boldsymbol{k}_1 \cdot diag(|\dot{\boldsymbol{q}}_e|)\boldsymbol{E}\right]\boldsymbol{J}^{-1}\boldsymbol{U}_2 - \frac{1}{2}\boldsymbol{x}\cdot\boldsymbol{k}_1 \cdot diag(|\dot{\boldsymbol{q}}_e|)\boldsymbol{L}\right. \\
&\quad \left. + \frac{1}{2}\boldsymbol{x}\left[m\boldsymbol{k}_2 diag(|\boldsymbol{q}_e^{m-1}|)\dot{\boldsymbol{q}}_e + n\boldsymbol{k}_3 diag(|\boldsymbol{q}_e^{n-1}|)\dot{\boldsymbol{q}}_e\right]\right\} \\
&\le \boldsymbol{S}^T\left\{\left[\boldsymbol{E}_4 + \boldsymbol{x}\cdot\boldsymbol{k}_1 \cdot diag(|\dot{\boldsymbol{q}}_e|)\boldsymbol{E}\right]\boldsymbol{J}^{-1}\boldsymbol{J}\left[\boldsymbol{E}_4 + \boldsymbol{x}\cdot\boldsymbol{k}_1 \cdot diag(|\dot{\boldsymbol{q}}_e|)\boldsymbol{E}\right]^{-1}\right. \\
&\quad \left\{\frac{1}{2}\boldsymbol{x}\cdot\boldsymbol{k}_1 \cdot diag(|\dot{\boldsymbol{q}}_e|)\boldsymbol{L} - \frac{1}{2}\boldsymbol{x}\left[m\boldsymbol{k}_2 diag(|\boldsymbol{q}_e^{m-1}|)\dot{\boldsymbol{q}}_e + n\boldsymbol{k}_3 diag(|\boldsymbol{q}_e^{n-1}|)\dot{\boldsymbol{q}}_e\right]\right. \\
&\quad \left.\left.-\left[\boldsymbol{k}_4 sig^{2k_5}(\boldsymbol{S}) + \boldsymbol{k}_6 sig^{2k_7}(\boldsymbol{S})\right]^q\right\}\right. \\
&\quad \left.-\frac{1}{2}\boldsymbol{x}\cdot\boldsymbol{k}_1 \cdot diag(|\dot{\boldsymbol{q}}_e|)\boldsymbol{L} + \frac{1}{2}\boldsymbol{x}\left[m\boldsymbol{k}_2 diag(|\boldsymbol{q}_e^{m-1}|)\dot{\boldsymbol{q}}_e + n\boldsymbol{k}_3 diag(|\boldsymbol{q}_e^{n-1}|)\dot{\boldsymbol{q}}_e\right]\right\} \\
&\le -\boldsymbol{S}^T\left[\boldsymbol{k}_4 sig^{2k_5}(\boldsymbol{S}) + \boldsymbol{k}_6 sig^{2k_7}(\boldsymbol{S})\right]^q \\
&\le -\left\{\boldsymbol{k}_4(\boldsymbol{S}^T\boldsymbol{S})^{k_5+0.5} + \boldsymbol{k}_6(\boldsymbol{S}^T\boldsymbol{S})^{k_7+0.5}\right\}^q
\end{aligned}$$

(40)

$$\leq -\left\{\sqrt{2}\boldsymbol{k}_4 diag(2^{k_5})(\frac{1}{2}\boldsymbol{S}^T\boldsymbol{S})^{k_5+0.5} + \sqrt{2}\boldsymbol{k}_6 diag(2^{k_7})(\frac{1}{2}\boldsymbol{S}^T\boldsymbol{S})^{k_9+0.5}\right\}^q$$
$$\leq -\left\{\tau_1(V)^{k_5+0.5} + \tau_2(V)^{k_7+0.5}\right\}^q$$
$$\leq -\left\{\tau_1(V)^{k_5'} + \tau_2(V)^{k_7'}\right\}^q$$

According to Lemma 1, the convergence time can be determined as:

$$T \leq \frac{1}{\tau_1^{\,q}(1-k_5^{'}q)} + \frac{1}{\tau_2^{\,q}(k_7^{'}q-1)} \tag{41}$$

3.3. Controller design of the rotating appendage

For the rigid rotating appendage, a rigid rotating payload is installed in the *x*-axis direction of the spacecraft platform. Similarly, we propose an appropriate control scheme to ensure a stable rotation, as follows:

$$\boldsymbol{S}_{pe} = \boldsymbol{\omega}_{pe} + sig(\boldsymbol{k}_{p1} * sig^2(\dot{\boldsymbol{q}}_{pe}) + \boldsymbol{k}_{p2} * \boldsymbol{q}_{pe}^{\ a} + \boldsymbol{k}_{p3} * \boldsymbol{q}_{pe}^{\ b})^c, \tag{42}$$

where $\boldsymbol{k}_{p1}$, $\boldsymbol{k}_{p2}$, and $\boldsymbol{k}_{p3}$ are the parameter matrices, and $\boldsymbol{k}_{p1}$=diag(k_{p11},k_{p12},k_{p13}), $\boldsymbol{k}_{p2}$=diag(k_{p21},k_{p22},k_{p23}), and $\boldsymbol{k}_{p3}$=diag(k_{p31},k_{p32},k_{p33}), where $ac<1$, and $bc>1$.

The corresponding control law can be expressed as follows:

$$\begin{aligned}\boldsymbol{U}_p = \boldsymbol{I}_P \Bigg\{ & -\frac{1}{2} diag(\left|\boldsymbol{k}_{p1} sig^2(\dot{\boldsymbol{q}}_{pe}) + \boldsymbol{k}_{p2}\boldsymbol{q}_{pe}^a + \boldsymbol{k}_{p3}\boldsymbol{q}_{pe}^b\right|^{c-1})\Big[2\boldsymbol{k}_{p1} diag(\left|\dot{\boldsymbol{q}}_{pe}\right|)\ddot{\boldsymbol{q}}_{pe} \\ & + a\boldsymbol{k}_{p2} diag(\left|\boldsymbol{q}_{pe}\right|^{a-1})\dot{\boldsymbol{q}}_{pe} + b\boldsymbol{k}_{p3} diag(\left|\boldsymbol{q}_{pe}\right|^{b-1})\dot{\boldsymbol{q}}_{pe}\Big] \\ & -\left[\boldsymbol{k}_{p4} sig^{2k_{p5}}(\boldsymbol{S}) + \boldsymbol{k}_{p6} sig^{2k_{p7}}(\boldsymbol{S})\right]^c\Bigg\} - \boldsymbol{T}_c + \tilde{\boldsymbol{\omega}}_p \boldsymbol{I}_P \boldsymbol{\omega}_p\end{aligned} \tag{43}$$

The Lyapunov analysis and proof are the same as that described in Section 3.2, which is omitted here.

4. Numerical simulation results

This study focuses on the attitude control of a new type of rotating satellite connected to the spacecraft platform and the rotating payload via frictionless magnetic bearings. The performance of proposed fixed-time sliding mode controller is demonstrated in this section. The results of the proposed method are compared with those of the proportional derivative (PD) controller. In numerical simulation,

the first four modes of vibration were considered for flexible solar panels, and the parameters of the spacecraft platform, flexible solar panels, magnetic bearing, and rotating payload were set as follows:

$$\boldsymbol{I}_{b0}=diag\left(4938.75,4642.63,6607.31\right)Kg\cdot m^2,\ I_{a0}=193.75Kg\cdot m^2$$

$$\boldsymbol{I}_{p0}=diag\left(251.78,0.79,0;0.79,15.76,0.32;0,0.32,11.46\right)Kg\cdot m^2$$

$$f_{sa1}=\begin{bmatrix}1.996e-9 & \text{-}1.425e1 & 8.016e-10\\ -2.451e-2 & -2.016 & 5.946e-3\\ 14.5 & 1.916e-8 & 6.824e-10\end{bmatrix},\quad f_{sa2}=\begin{bmatrix}-15.0146 & \text{-}2.125e-8 & 2.616e-8\\ -2.451 & 2.516e-3 & 4.346e-8\\ 2.143e-10 & 16.16 & 2.124e-6\end{bmatrix}$$

$$f_{sa3}=\begin{bmatrix}-2.842e-7 & 8.164e-3 & -1.921e-8\\ 1.274e-3 & 9.524e-3 & -2.014\\ -8.302e-5 & -2.840e-7 & -1.56e-8\end{bmatrix},\ f_{sa4}=\begin{bmatrix}-1.519e-8 & 3.441 & 2.502e-9\\ 1.376e-2 & -0.546 & -3.014e-3\\ -3.412 & -5.840e-7 & 2.021e-7\end{bmatrix}$$

$$\boldsymbol{F}_a=\begin{bmatrix}-1.9e1 & -3.11e-9 & -1.58e-2 & 2.984e-1 & -1.0287 & 3.945e-3\\ 1.38e-2 & 8.98e-6 & -3.214 & 5.08e-2 & 5.982e-3 & 1.174\\ 2.91e-6 & -1.913 & -5.07e-6 & 3.13e-8 & 2.06e-7 & -5.09e-6\end{bmatrix}$$

$$r_{sa1}=\begin{bmatrix}5.996e-8 & 0 & 6.213e-4\\ 0 & 4.88e1 & 1.613e-9\\ -3.75e2 & 0 & 1.216e-6\end{bmatrix},\ r_{sa2}=\begin{bmatrix}-1.329e-6 & 0 & -1.717e-1\\ 0 & -8.964e-4 & 0\\ 1.826e-3 & 1.023e-7 & 1.071e-6\end{bmatrix}$$

$$r_{sa3}=\begin{bmatrix}3.462e1 & 0 & -1.213e-5\\ 0 & 1.011 & 0\\ -4.956e-6 & 0 & 9.016e-2\end{bmatrix}$$

In this analysis, the mass of the spacecraft platform was 1850 kg, and that of the rotating payload was 900 kg. The initial angular velocity of the platform was $\boldsymbol{\omega}_{b0}=\left[0.03;0.01;0.04\right]\ rad/s$, that of the flexible solar panels relative to the platform was $\omega_{ay}=0.05\ rad/s$, and that of the rotating payload was $\boldsymbol{\omega}_{p0}=\left[0.1;0;0\right]\ rad/s$. The desired angular velocity of the platform was $\boldsymbol{\omega}_{bd}=\left[0;0;0\right]\ rad/s$, that of flexible solar panels was $\omega_{ad}=0.1\ rad/s$, and that of the rotating payload around the *x*-axis of the platform was $\boldsymbol{\omega}_{pd}=\left[0.2;0;0\right]\ rad/s$. The external disturbance torque, which included constant and period disturbances, was defined as $\boldsymbol{d}=[\sin(0.13\pi t)+1;\sin(0.13\pi t)+1;\sin(0.13\pi t)+1]$. The parameters of the controller were selected as follows:

$$\boldsymbol{c}_1 = diag(5,5,5), \boldsymbol{c}_2 = diag(105,100,100), \boldsymbol{c}_3 = diag(100,100,100),$$
$$\boldsymbol{k}_\alpha = diag(-20,-20,-20), \boldsymbol{k}_\beta = diag(-1,-1,-1), k_i = 12.02, k_x = 37,$$
$$\boldsymbol{k}_1 = diag(320,320,320,180), \boldsymbol{k}_2 = diag(200,200,200,75),$$
$$\boldsymbol{k}_3 = diag(640,720,640,580), \boldsymbol{k}_4 = diag(0.009,0.005,0.004,0.008), m = 1,$$
$$\boldsymbol{k}_6 = diag(0.0075,0.008,0.005,0.006), n = 1.2, q = 0.5,$$
$$\boldsymbol{k}_{p1} = diag(1,1,1), \boldsymbol{k}_{p2} = diag(21,21,23),$$
$$\boldsymbol{k}_{p3} = diag(12,12,12), a = 1, b = 1.5, c = 0.5$$

Figures 4 and 5 present the results of the attitude angular velocity and the vector of the error quaternion of the platform. Figure 6 shows the results of the attitude angular velocity error of flexible solar panels relative to the *y*-axis of the spacecraft platform. Figure 7 shows the angular velocity error of the payload rotating about the *x*-axis of the spacecraft platform. Figure 8 shows the variation trend of the magnetic gap error of the magnetic bearing.

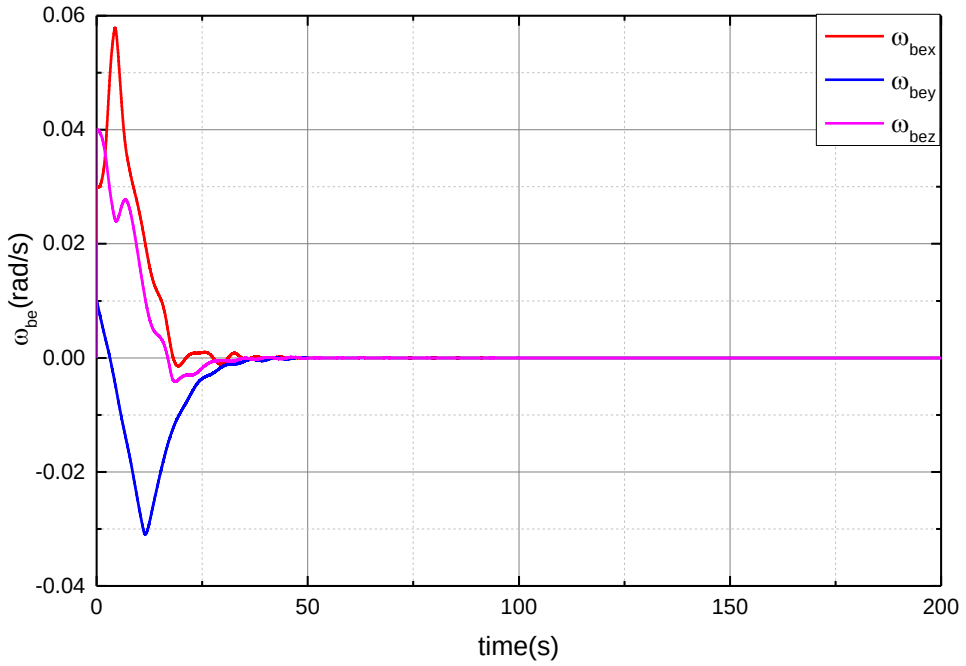

Figure 4. error angular velocity variation of spacecraft platform.

In terms of the stability time of the spacecraft system, the maglev bearing is the first to reach a stable state, after which the rotating payload, spacecraft platform, and flexible solar panels reach their desired states. The angular velocity and quaternion errors of the spacecraft platform, attitude angular velocity error of flexible solar panels, and payload converge to stable states in less than the theoretical time. The theoretical time of the magnetic gap error of the magnetic bearing is less than that of the other components of the spacecraft system. It can be shown that the control law proposed in this paper ensures that the components of the spacecraft system converge to the equilibrium position in a fixed theoretical time, and it can be shown that the law is useful and effective.

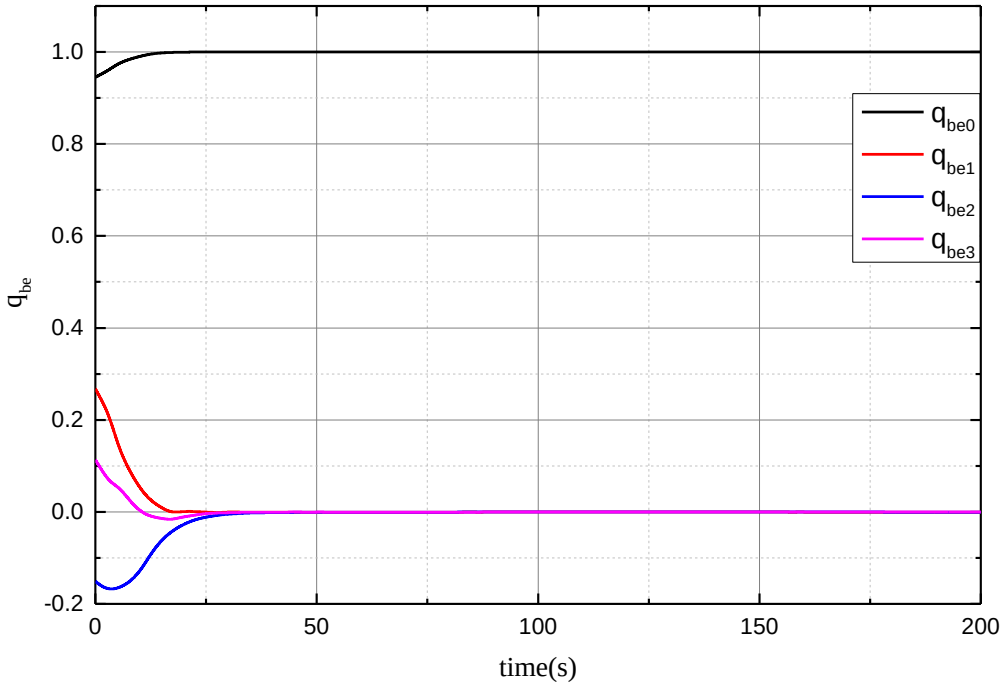

Figure 5. error quaternion variation of spacecraft platform.

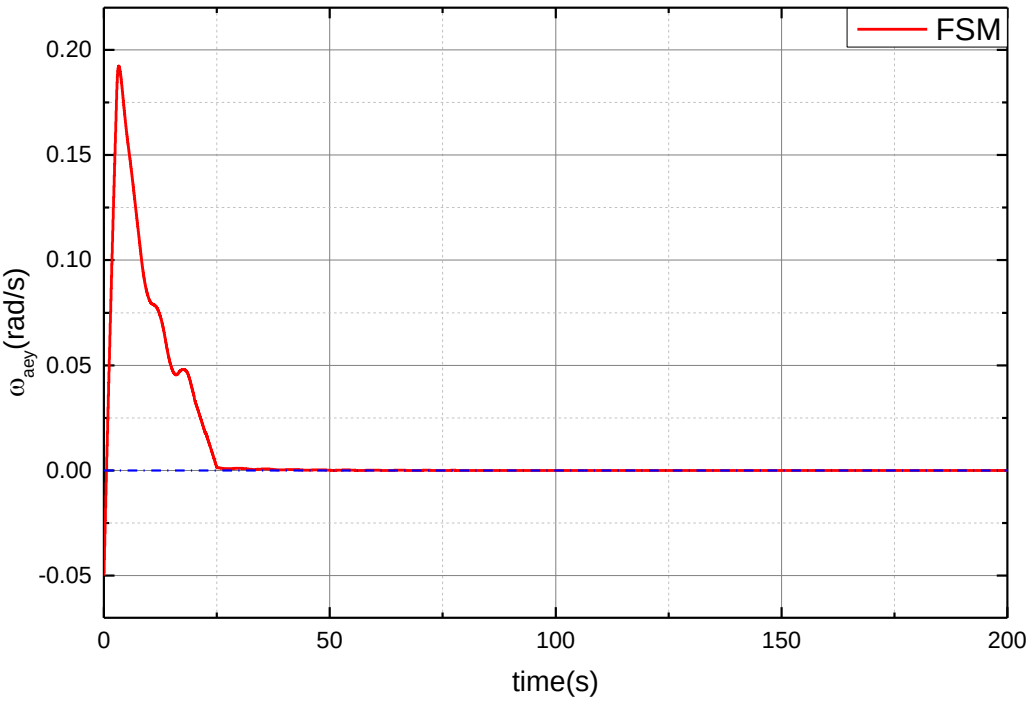

Figure 6. error angular velocity variation of flexible solar panels.

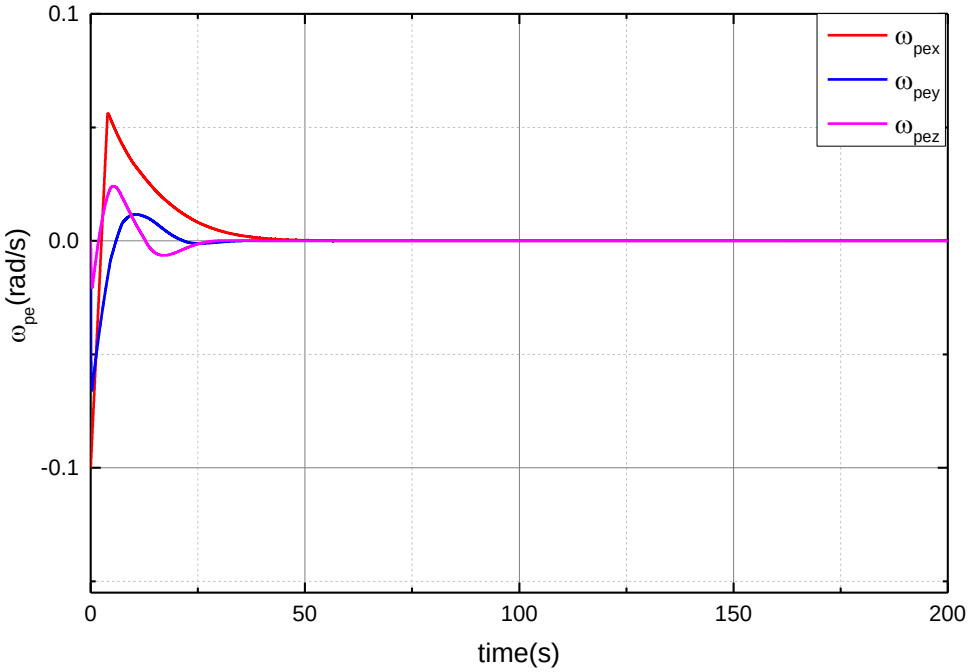

Figure 7. error angular velocity variation of rotating payload.

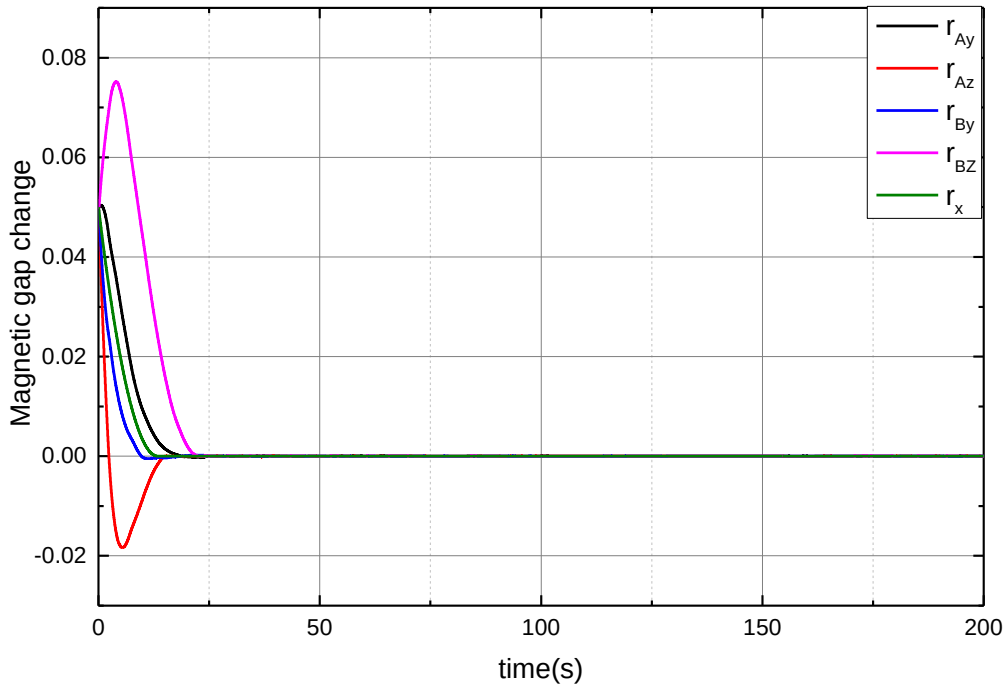

Figure 8. magnetic gap variation of active maglev bearing.

Figures 9 and 10 show the angular velocity and quaternion errors of the spacecraft platform obtained using our finite state machine (FSM) control scheme; the results converge better than those

obtained using the existing control PD scheme. The control law proposed in this paper requires 35 s for the angular velocity and error quaternion errors to converge to the equilibrium position, whereas the PD algorithm requires approximately 150 s.

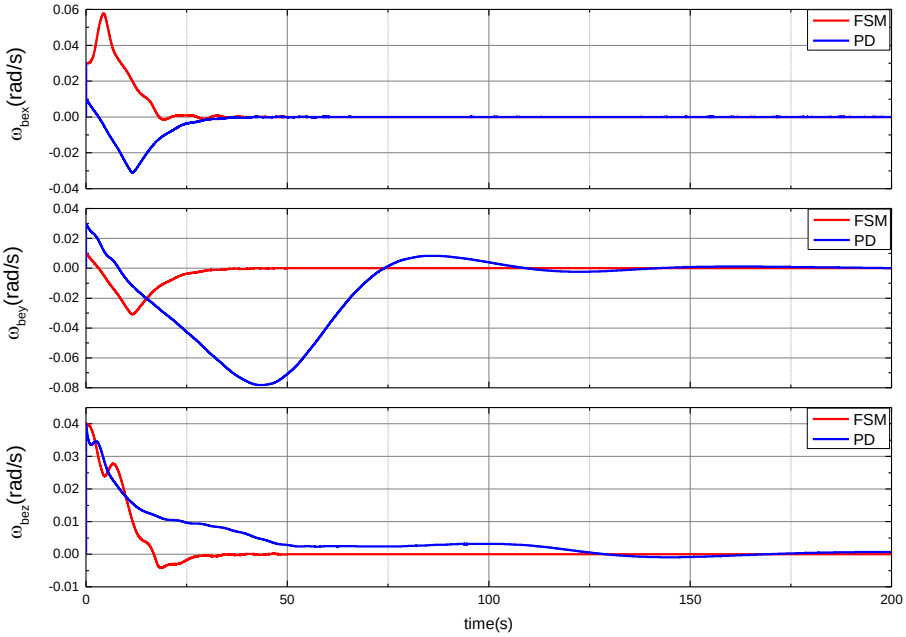

Figure 9. Comparisons of spacecraft platform error angular velocity.

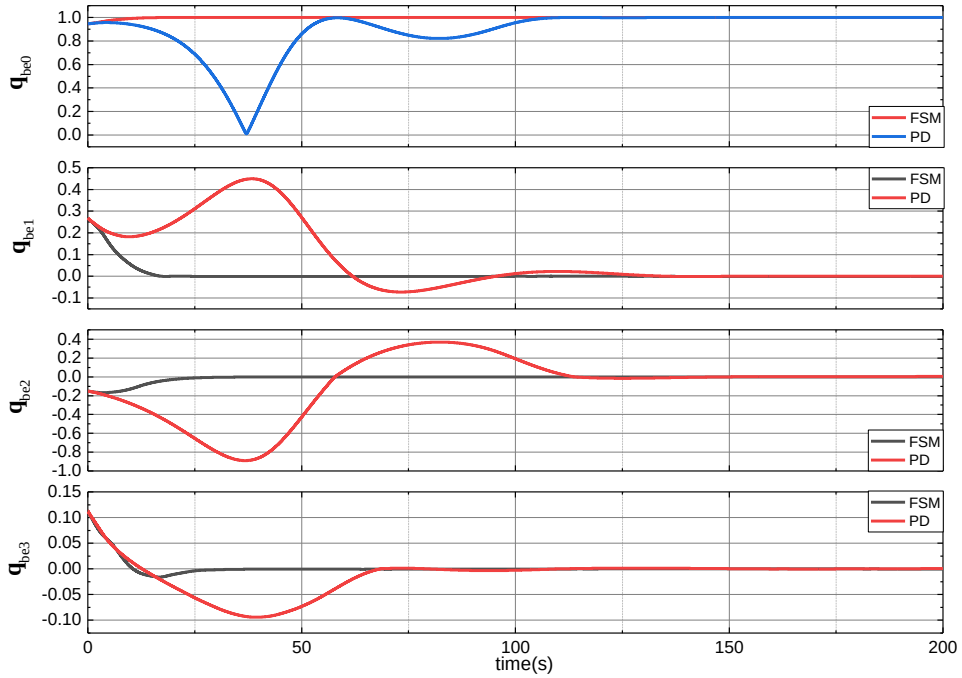

Figure 10. Comparisons of spacecraft platform error quaternion.

Figure 11 shows the change in the angular velocity error of the flexible solar panels relative to the *y*-axis rotation of the spacecraft platform under different control laws. The FSM law can make the

flexible solar panels rotate stably in 30 s, whereas the PD control law takes approximately 100 s.

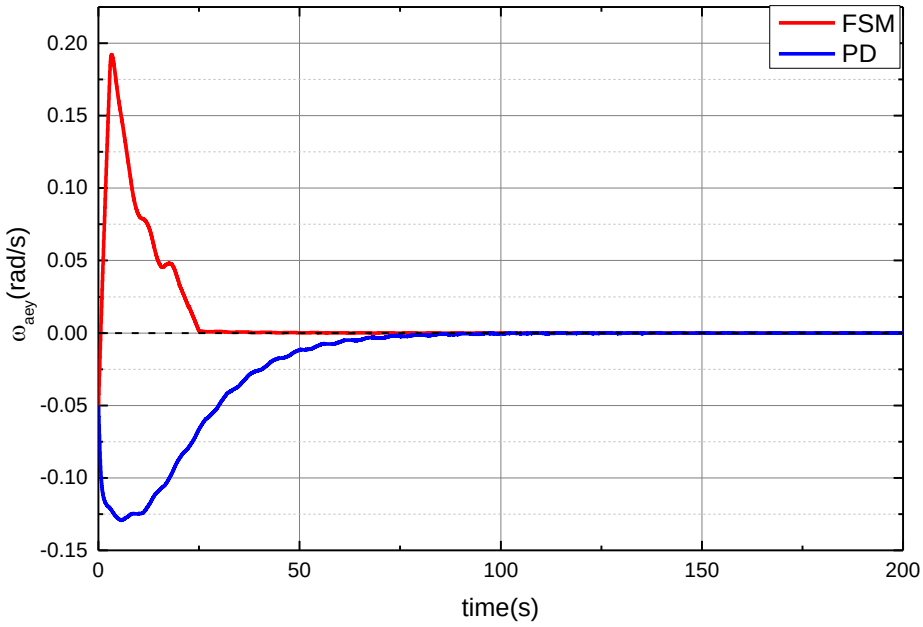

Figure 11. Comparisons of flexible solar panels error angular velocity.

Figure 12 shows the angular velocity error of the rotating payload from the static state to the stable state under different control laws. It can be seen that the convergence time of the PD control law is longer than that of the FSM control law.

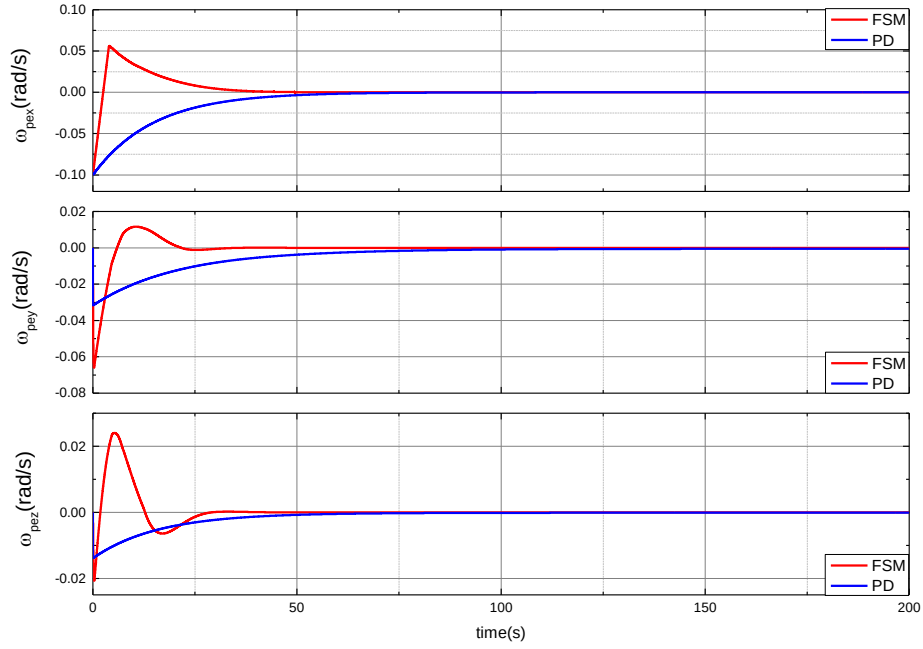

Figure 12. Comparisons of rotating payload error angular velocity.

Figure 13 shows the error gap of the magnetic bearing under different control laws. As shown, the convergence time of the FSM law is approximately 25 s. Thus, it can be concluded that the proposed FSM provides faster convergence than the PD control scheme. In terms of the stability time of the spacecraft system, the maglev bearing is the first to reach a stable state, after which the rotating payload, spacecraft platform, and flexible solar panels reach their desired states.

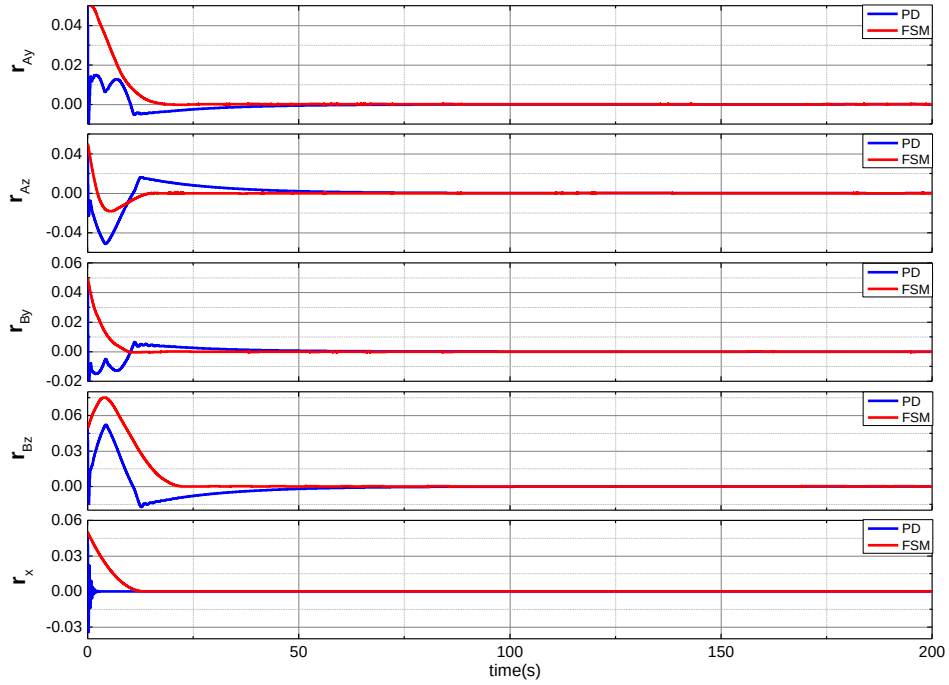

Figure 13. Comparisons of magnetic gap of active maglev bearing.

5. Conclusion

In this study, a dynamic model of a spacecraft with a rotating payload and rotating flexible solar panels was established. To realize the rotation of the rotating payload and flexible solar panels relative to the spacecraft platform at a predefined angular velocity, we proposed a fixed-time control scheme whose convergence time was independent of the initial information of the spacecraft system based on the existing controller. The control laws provided rapid convergence and accurate performance in the presence of disturbances. Moreover, illustrative numerical simulations demonstrated the spacecraft could effectively track its desired attitude. The simulation results showed that the attitude of the spacecraft system converged to a small neighborhood near the stabilized state in a fixed time. However, our study suggests that there is a difference between the actual application and our assumptions, making it important to consider the actual maximum allowable torque. Consequently, the attitude control problem of the payload actuator failure based on the proposed laws will be our next focus, and we expect our study to provide references for the attitude control system to ensure the completion of the observation mission in the future.

Data availability

The data used to support the findings of this study are included within this paper.

Conflicts of interest

The authors declare that there is no conflict of interest regarding the publication of this paper.

Acknowledgements

This work is supported by the Science Center Program of National Natural Science Foundation of China (Grant No.62188101), the National Natural Science Foundation of China (Grant No. 61833009, 61690212, 11972130), the Heilongjiang Touyan Team, and the Guangdong Major Project of Basic and Applied Basic Research (Grant No. 2019B030302001).

References

1. Z. Wang, D. Yang, H. Zhang, Stability analysis on a class of nonlinear fractional-order systems, *Non. Dyn.,* **86** (2016), 1023–1033. doi: 10.1007/s11071-016-2943-6.
2. J. Pongfai, X. Su, H. Zhang, W. Assawinchaichot, PID controller autotuning design by a deterministic Q-SLP algorithm, *IEEE Access*, **8** (2020), 50010–50021. doi: 10.1109/ACCESS.2020.2979810.
3. Q. Zhou, H. Li, C. Wu, L. Wang, C. K. Ahn, Adaptive fuzzy control of nonlinear systems with unmodeled dynamics and input saturation using small-gain approach, *IEEE Trans. Syst. Man Cybern*, **47** (2017), 1979–1989. doi: 10.1109/TSMC.2016.2586108.
4. N. Wang, Y. Gao, Z. Sun, Z. Zheng, Nussbaum-based adaptive fuzzy tracking control of unmanned surface vehicles with fully unknown dynamics and complex input nonlinearities, *Int. J. Fuzzy Syst.*, **20** (2018), 259–268. doi: 10.1007/s40815-017-0387-x.
5. H. Schättler, U. Ledzewicz, B. Cardwell, Robustness of optimal controls for a class of mathematical models for tumor anti-angiogenesis, *Math. Biosci. Eng.,* **8** (2011), 355–369. doi: 10.3934/mbe.2011.8.355.
6. J. Jang, K. Jang, H. Kwon, J. Lee, Feedback control of an HBV model based on ensemble kalman filter and differential evolution, *Math. Biosci. Eng.*, **15** (2018), 667–691. doi: 10.3934/mbe.2018030.
7. L. Chen, Y. Zhu, C. K. Ahn. Adaptive neural network-based observer design for switched systems with quantized measurements, *IEEE Trans. Neural Netw. Learn Syst.*, (2021). doi: 10.1109/TNNLS.2021.3131412.
8. P. Li, Z. Lin, H. Shen, Z. Zhang, Optimized neural network based sliding mode control for quadrotors with disturbances, *Math. Biosci. Eng.*, **18** (2021), 1774–1793. doi: 10.3934/mbe.2021092.
9. W. Qi, G. Zong, H. R. Karimi, Sliding mode control for nonlinear stochastic singular semi-markov jump systems, *IEEE Trans. Automat. Contr.*, **65** (2020), 361–368. doi: 10.1109/TAC.2019.2915141.
10. M. Liu, L. Zhang, P. Shi, Y. Zhao, Fault estimation sliding mode observer with digital communication constraints, *IEEE Trans. Automat. Contr.*, **63** (2018), 3434–3441. doi: 10.1109/TAC.2018.2794826.
11. X. Gu, X. Tong, Overview of china earth observation satellite programs, *IEEE Geosci. Remote Sens. Mag.*, **3** (2015), 113–129. doi: 10.1109/MGRS.2015.2467172.

12. A. T. A. Peijnenburg, J. P. M. Vermeulen, J. van Eijk, Magnetic levitation systems compared to conventional bearing systems, *Microelectron*, **83** (2006), 1372–1375. doi: 10.1016/j.mee.2006.01.248.
13. Y. Li, X. Wang, X. Xie, D. Gu, C. Dong, Study on the control of the adaptive PID of the model of uncertain magnetic suspension bearings, *J. Anhui University Sci. Tech.*, **38** (2018), 44–47. doi: 10.3969/j.issn.1672-1098.2018.02.008.
14. I. S. Kuseyri, Robust control and unbalance compensation of rotor/active magnetic bearing systems, *J. Vib. Contr.*, **18** (2012), 817–832. doi: 10.1177/1077546310397560.
15. X. Cao, P. Shi, Z. Li, M. Liu, Neural-network-based adaptive backstepping control with application to spacecraft attitude regulation, *IEEE Trans Neural Netw. Learn Syst.*, **29** (2017), 4303–4313. doi: 10.1109/TNNLS.2017.2756993.
16. M. S. Kang, J. Lyou, J. K. Lee, Sliding mode control for an active magnetic bearing system subject to base motion, *Mechatronics*, **20** (2010), 171–178. doi: 10.1016/j.mechatronics.2009.09.010.
17. D. Zhang, X. Fang, X. Zhang, H. Wu, L. Zhang, Terminal sliding mode variable structure control of active magnetic bearing, *J. Wuhan Uni.*, **52** (2019), 736–740. doi：10.14188/j.1671-8844.2019-08-012.
18. F. Wu, X. Cao, E.A. Butcher, F. Wang, Dynamics and control of spacecraft with a large misaligned rotational component, *Aero. Sp. Sci. Technol.*, **87** (2019), 207–217. doi: 10.1016/j.ast.2019.02.029.
19. D. Zhao, Y. Zhong, L. Wu, Y. Fang, Modeling and design of a novel permanent-magnet biased 3-DOF magnetic bearing, *Sm. Sp. Elec. Mac.*, **47** (2019), 5–9. doi: 10.3969/j.issn.1004-7018.2019.07.002.
20. Y. Zhao, X. Chen, F. Wang, C. Wei. Y. Zhao, Modeling of active magnetic bearing in rotating payload satellite considering shaft motion coupling, *J. Mech. Sci. Technol.*, **34** (2020), 4423–4437. doi: 10.1007/s12206-020-1005-7.
21. M. J. Sidi, Spacecraft dynamics and control: A practical engineering approach, C*ambridge University Press, Cambridge*, (1997). doi: 10.2514/2.3299.
22. G. Zhang, X. Chen, R. Xi, H. Li, Nonsingular integral sliding mode attitude control for rigid-flexible coupled spacecraft with high-inertia rotating appendages, *Complexity*, **1** (2021), 1–17. doi: 10.1155/2021/8812187.
23. Y. Miao, I. Hwang, M. Liu, F. Wang, Adaptive fast nonsingular terminal sliding mode control for attitude tracking of flexible spacecraft with rotating appendage, *Aero. Sp. Sci. Technol.*, **93** (2019), 1–10. doi: 10.1016/j.ast.2019.105312.
24. X. Song, Y. Chen, Control and simulation of spacecraft's attitude control based on quaternions, *Appl. Mech. Mater.*, **380–384** (2013), 298–301, doi: 10.4028/www.scientific.net/AMM.380-384.298.
25. B. Xiao, Q. Hu, Y. Zhang, Adaptive sliding mode fault tolerant attitude tracking control for flexible spacecraft under actuator saturation, *IEEE Trans. Contr. Syst. Technol.*, **20** (2011), 1605–1612. doi: 10.1109/TCST.2011.2169796.
26. L. Lu, J. Fei, L. Yu, Y. Yuan, A rolling bearing fault detection method based on compressed sensing and a neural network, *Math. Biosci. Eng.*, **17** (2020), 5864–5882. doi: 10.3934/mbe.2020313.

27. D. Zhang, C. Huang, J. Fei, Defect reconstruction from magnetic flux leakage measurements employing modified cuckoo search algorithm, *Math. Biosci. Eng.*, **18** (2021),1898–1925. doi: 10.3934/mbe.2021099.
28. N. S. Gibson, G. D. Buckner, H. Choi, F. Wu, Confidence interval networks for bounding model uncertainty: experimental evaluations on an active magnetic bearing system//Soft Computing in Industrial Applications, *Pro. of the 2005 IEEE Mid-Summer Workshop on IEEE*, (2005). doi:10.1109/SMCIA.2005.1466966.
29. A. Jiang, Q. Hu, M. I. Friswell, Fixed-time attitude control for rigid spacecraft with actuator saturation and faults, *IEEE Trans. Contr. Syst. Technol.*, **24** (2016), 1892–1898. doi: 10.1109/TCST.2016.2519838.
30. Y. Guo, S. Song, Adaptive finite–time backstepping control for attitude tracking of spacecraft based on rotation matrix, *Chin. J. Aero.*, **27** (2014), 375–382. doi: 10.1016/j.cja.2014.02.017.
31. S. Yu, X. Yu, B. Shirinzadeh, Z. Man, Continuous finite-time control for robotic manipulators with terminal sliding mode, *Automat.*, **41** (2005), 1957–1964. doi: 10.1016/j.automatica.2005.07.001.
32. B. Liu, L. Ai-Jun, B. Huang, Attitude control of aerospace vehicle based on adaptive fixed-time sliding mode controller, *Comput. Sim.*, **36** (2019), 5–8. doi: 10.3969/j.issn.1006-9348.2019.11.004.
33. Y. Zhu, W. Zheng, Multiple lyapunov functions analysis approach for discrete-time switched piecewise-affine systems under dwell-time constraints, *IEEE Trans. Automat. Contr.*, **65** (2020), 2177–2184. doi: 10.1109/TAC.2019.2938302.